NOTICE CONCERNING COPYRIGHT RESTRICTIONS

CRUSTAL STRUCTURE IN NORTHERN NEVADA FROM SEISMIC REFRACTION DATA

by Douglas A. Stauber

U.S. Geological Survey
345 Middlefield Rd.
Menlo Park, CA 94025

Abstract

Three seismic refraction profiles were recorded in and around the Battle Mountain heat flow high in north-central Nevada. Models of P and S velocity structure derived from these profiles together with previously published profiles reveal a substantial variation in crustal thickness in this region (from 23 km to 35 km). The crust is thinnest in a band between the Battle Mountain-Winnemucca area and Reno, and thickens to the northwest, east and south. The expected gravity anomaly associated with the variation in crustal thickness matches the shape of the observed Bouger gravity field well, but acceptable fit to the gravity data requires either an unusually small density contrast (0.16 g/cm^3) between the crust and uppermost mantle or a partially compensating mass somewhere in the crust or upper mantle. A likely candidate for the latter option involves variation in the thickness of the lithosphere itself.

Introduction

Large amplitude long wavelength anomalies in the heat flow and gravity fields in northern Nevada as well as published seismic refraction work indicate significant lateral variations occur in the crust in this region. The Bouguer gravity field in northern Nevada, Figure 1, shows a large rectangular region of high values in northwestern Nevada corresponding to the Lake Lahonton topographic low and a gravity low over the topographically high region in the center of Nevada. Seismic P velocity models for two reversed refraction lines in northern Nevada have been published by Eaton (1963) and Hill and Pakiser (1966). Locations are shown as long-dashed lines in Figures 1 and 2. These models have a variation in crustal thickness of 10 km (24 to 34 km) with the thin crust occurring near Fallon, Nevada where the refraction line is in the gravity high. Several other unreversed refraction lines in northern Nevada, using nuclear tests occurring in southern Nevada as sources, have been interpreted for crustal thickness variations by Stauber and Boore (1978) and Priestly and others (1982). Locations of these profiles are shown with short dashed lines on Figures 1 and 2. These interpretations have a thin (20 to 24 km) crust in the region of the gravity high and a thick crust (30 to 35 km) under the gravity low in central Nevada. The interpretation of unreversed refraction lines is not unique so verification of these interpretations is necessary.

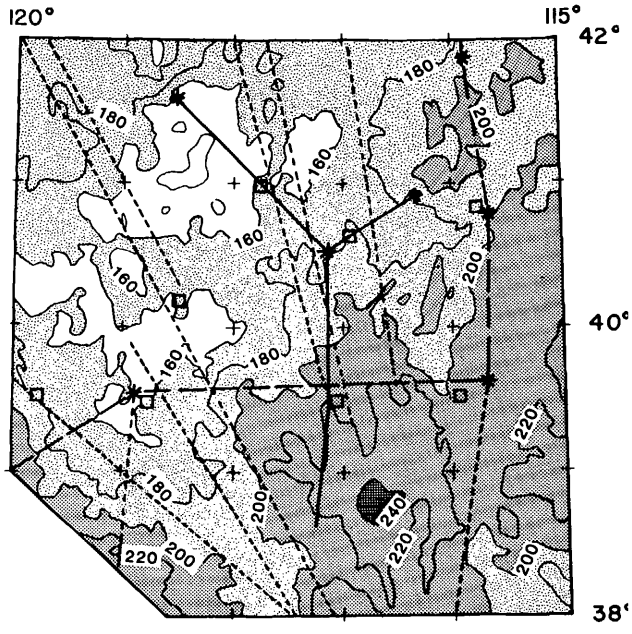

Figure 1. Locations of refraction lines in northern Nevada superimposed on Bouguer gravity map for the region from Eaton (1978). Gravity values are in mgal. Contour interval is 20 mgal. Solid lines are described in this paper. Long dashed lines are published reversed refraction lines and short dashed lines are published unreversed refraction lines. See figure 2 for references to published lines.

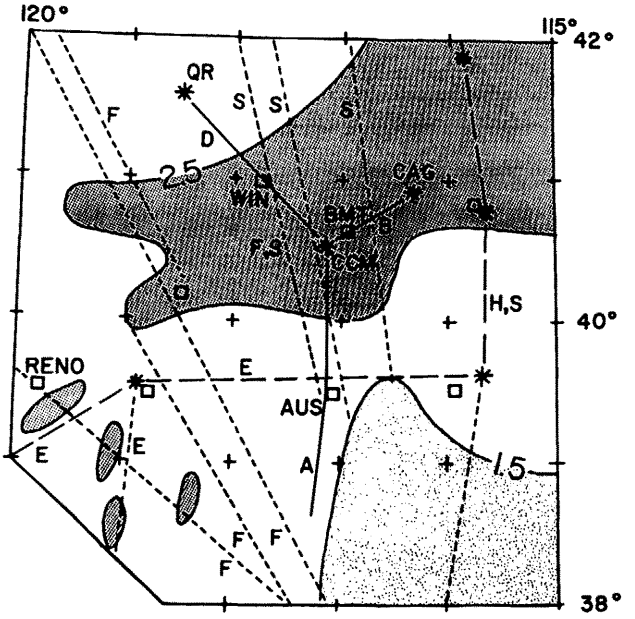

Figure 2. Locations of refraction lines superimposed on heat flow map of Lachenbruch and Sass (1978). Dark pattern shows the HFH where the conductive heat flow is greater than 100 mW/m^2. Light pattern shows location of heat flow low in central Nevada where heat flow is less than 60 mW/m^2. Place name abbreviations are; WIN=Winnemucca; BMT= Battle Mountain; AUS= Austin. Shot points are shown with stars. Key to refraction lines ; A,B,D are described in this paper; E = Eaton (1963); F = Priestley and others (1982); H = Hill and Pakiser (1967); S = Stauber and Boore (1978).

In addition to the large gravity anomalies and seismic velocity structures of northern Nevada, there is a large heat flow anomaly.

The Battle Mountain Heat Flow High, HFH, described by Lachenbruch and Sass (1978) is a large region in which the conductive heat flux is greater than 100 mW/m^2, compared to the more typical, but still high, Basin and Range values near 80 mW/m^2. The location of the HFH is shown in Figure 2 along with the published refraction line locations. Stauber and Boore (1978) noted a correlation in the position of the southern boundary of the HFH and the crustal thickness change, thinner within the HFH than to the south, on the four eastern north-south profiles. Partial melting in the crust of the HFH as well as the tectonic extension models of Lachenbruch and Sass (1978) could produce large variations in the seismic velocity structure of the crust and mantle in the HFH. More detailed, reversed refraction lines are required to search for these effects and to constrain the interpretation of the unreversed profiles.

Experiment Description

To accomplish these goals three detailed reversed refraction lines in north central Nevada were recorded and interpreted. The locations of these lines are shown in Figures 1 and 2 as solid lines. These lines span the HFH and the gravity anomalies discussed above. Regular quarry blasts at the Copper Canyon Mine (CCM), 40.54°N, 117.13°W, and at the Carlin Gold Mine (CAG), 41.61°N, 116.32°W, served as the primary sources for these detailed refraction lines. In addition, a 2000 lb shot detonated by the U. S. Geological Survey in northwestern Nevada near the Quinn River (QR), 41.61°N, 118.52°W, was recorded. Line A, running south from CCM was partially reversed by recordings of Nevada Test Site, NTS, events. Additionally, line A crosses the east-west reversed profile of Eaton (1963), which provided control for dip along line A. Line A crosses both the HFH boundary and the gravity anomaly. Line B, between CCM and CAG, is entirely within the HFH. Both shotpoints were recorded on this line. Reversed coverage on line D was obtained by recording both the QR and CCM shotpoints.

Recording was performed with several types of seismographs. Most of the detailed refraction lines were recorded with 5 portable analog FM recorders built at Stanford University (Stauber, 1980). The QR shot was also recorded with U. S. Geological Survey 5-day analog FM recorders (Criley and Eaton, 1978). Sprengnether MEQ-800 smoked paper recorders were used to record NTS events and as reference stations on lines A and B. 1 Hz geophones were used as sensors for all the recording systems.

Recording site spacing of 2 to 10 km was obtained with 5 recorders by moving the recorders along the lines and recording many blasts. One smoked drum station remained fixed at a "reference" site to obtain shot time and amplitude information. For each reference site, a few shots at the appropriate quarry were recorded with a geophone at the edge of the shot hole pattern to provide an accurate shot time and travel time to the reference site. For subsequent shots, the arrival time measured at the reference station was used to obtain shot time and corrections for small shot location changes in the large quarries by the method described by Stauber (1980). Amplitudes of the P waves were measured from the reference records and used to correct for shot size varations in the record sections on Lines B and D (Stauber, 1980). Because of variation in waveform of different shots and instrumental variations, the amplitude normalization is considered accurate within a factor of 2. No amplitude normalization was attempted for line A because several reference sites were used at various

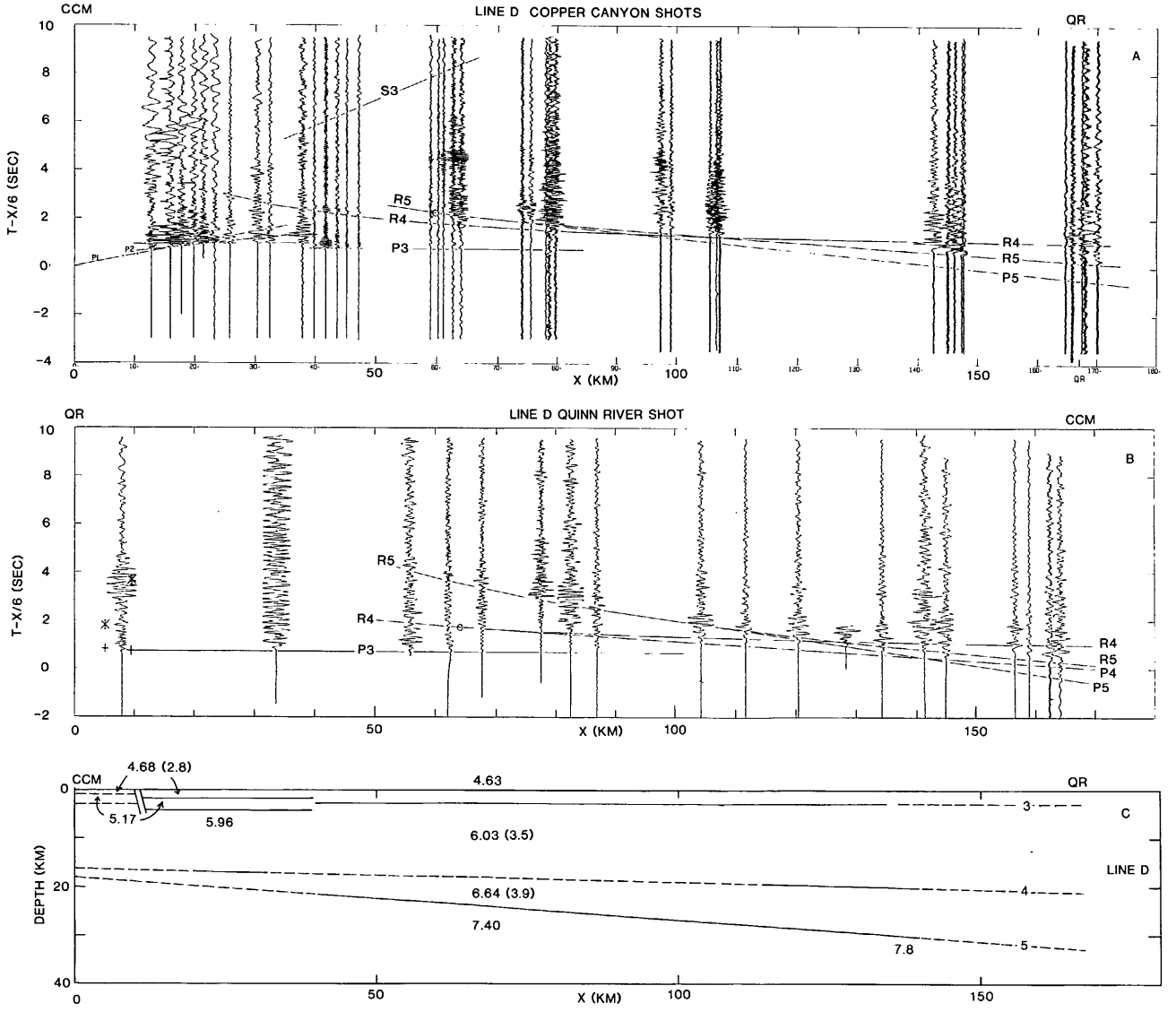

Figure 3. A) Vertical component record section for CCM shots on line D. Travel-time curves are computed from model in figure 3C. B) Vertical component record section for QR shot on line D.
C) Velocity model for line D. P velocities and S velocities (in parenthesis) are in km/sec. The solid portions of the interfaces in the model indicate the parts of the interfaces for which observations of refracted and reflected waves exist.

times on this line. Vertical component record sections for lines D, B and A with reducing velocity of 6.0 km/sec are shown in Figures 3, 5 and 7.

First motion times and amplitudes were measured on the record section for all recordings where it was possible. For some of the weaker signals, a tracing of a clearer example at a nearby station was overlayed on the weak trace and used to estimate the first motion time. An uncertainty was assigned to each measurement as it was made. Later phases were also identified on all the record sections. In identifying the later phases I relied mainly on an abrupt (within one cycle) increase in signal amplitude as well as coherence across more than three or four records. I was further biased

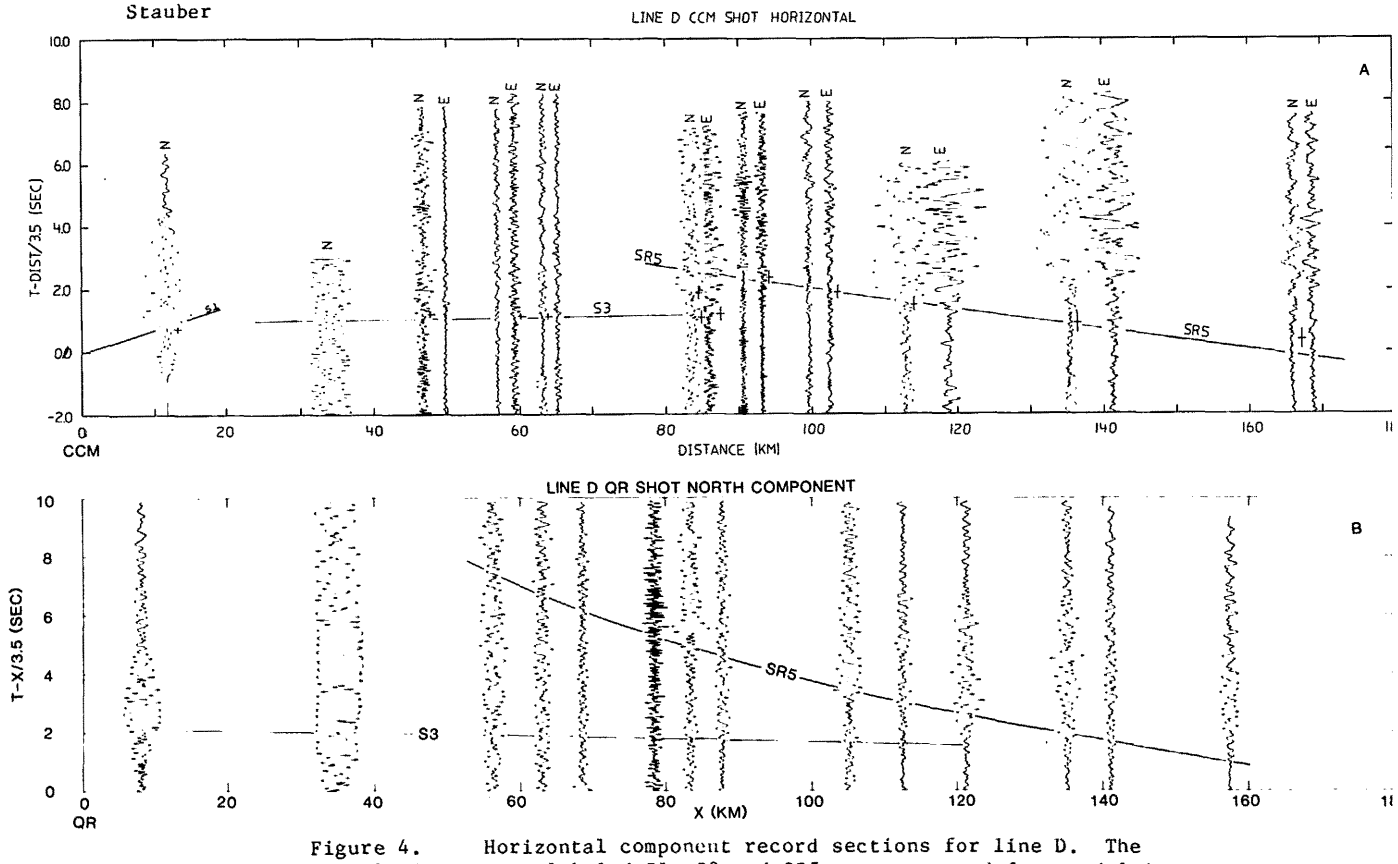

Figure 4. Horizontal component record sections for line D. The travel-time curves labeled S1, S3 and SR5 were computed from model in figure 3C. Section A is for CCM shots. The traces labeled N and E are north and east components. Section B is for the QR shot.

toward phases which could be fit by smooth traveltime curves such as those produced by refractions and reflections from planar portions of interfaces. Finally, since many shots were used on each line, I required that later phases be seen on records from several shots before considering them significant. Arrival times and amplitudes were measured and assigned an uncertainty for these later phases. A scatter of arrival times of $\pm$ 0.1 sec about potential smooth traveltime curves was commonly found for these later phases.

Shear waves were observed on all the lines and identified as such by their phase velocities, less than 4.5 km/sec. Record sections with a reducing velocity of 3.5 km/sec were produced to enhance the visibility of S waves for several vertical and horizontal component profiles. They are shown in Figures 4, 6 and 7.

Interpretation of Seismic Refraction Data

The seismic velocity structure along the lines was modeled as uniform velocity layers separated by planar dipping interfaces. Slightly more complicated structure was allowed near the surface to account for the alluvial filled basins crossed by the profiles. The dipping layer models were fit to the observed travel times by an iterative weighted, least-squares inversion program (Stauber, 1980). The reciprocals of the uncertainties in the measurements were used as weights so that poorly determined observations had only a weak influence on the model compared to well determined observatons. The S wave observations formed a less complete set of phases than the P wave observations. Consequently S wave velocities were obtained for the models by keeping the layer boundaries fixed at the positions determined by the P wave travel times and then solving for the S velocities within the layers with the same inversion program. Having discussed the data reduction and the interpretative method, we can proceed to discuss the results for the individual lines.

Line D is the longest, most fully reversed profile. Travel times from the dipping layer model, shown in Figure 3C, are plotted on the record sections in Figure 3 and 4. The first P arrivals near CCM, Figure 3A, are explained by three layers with velocities of 4.68, 5.17 and 5.96 km/sec as depth increases. 11 km northwest of CCM, Figuer 3A, the profile crosses from a range into a basin and the first arrivals are delayed by 0.10 to 0.14 sec. Assuming a valley fill with a velocity of 2.0 km/sec this corresponds to a fill thickness of 0.22 to 0.30

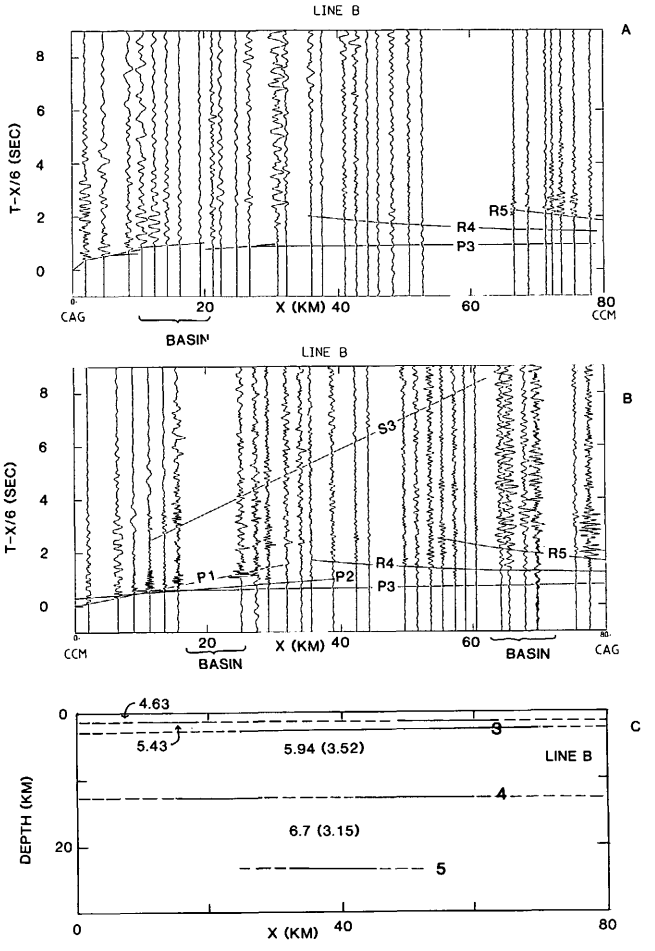

Figure 5. Vertical component record sections for line B. Section A is for CAG shots and section B is for CCM shots. Travel-time curves are computed from the model in figure 5C. P and S (in parenthesis) velocities in figure 5C are in km/sec.

km. At 40 km the first arrivals are offset about 0.2 sec. This corresponds to a lateral offset in the recording locations. The two segments, less than 40 km and more than 40 km, are radial to CCM but are about 15° apart in azimuth. This offset represents a lateral variation in the near surface structure. First arrivals from 40 to 90 km and from 0 to 90 km for the QR shot define apparent velocities of 6.0 km/sec. The phases marked R4 on the CCM and QR record sections are interpreted as reflections from the top of the 6.64 km/sec layer, the fourth interface in the model. These reflections control the position of the top of this layer. The phases marked R5 are interpreted as reflections from the bottom of this layer, the fifth interface of the model. The portion of these phases at large distance controls the velocity (6.64 km/sec) in the layer and the nearer shot portions control the depth to the base. Small first arrivals near 160 km for the QR shot in Figure 3B are interpreted as refracted waves from below the 6.64 km/sec layer. Using this interpretation, one obtains a velocity of 7.4 km/sec below the fifth interface.

S waves were also observed and modeled on line D. For the CCM shot, Figure 3A, a clear impulsive low frequency (2-5 hz) phase labeled S3 with an apparent velocity of 3.5 km/sec is visible between 35 and 65 km. Record sections for horizontal components recorded on Line D from both shotpoints are plotted with a reducing velocity of 3.5 km/sec in Figure 4.

For the QR shotpoint, Figure 4B, a tenuous phase (labeled S3) with an apparent velocity of 3.5 km/sec and an intercept time near 2 seconds is seen. A reflected phase, SR5, is clearly visible, particularly at larger distances. For the reverse direction, at CCM shotpoint in Figure 4A, low frequency S3 and SR5 phases are again visible. Assuming that these S phases were generated at the source, and holding the layer boundares fixed in the positions determined by the P waves, the S velocities of the layers were found by the least square inverse program and are plotted, in parenthesis on the model for line D, Figure 3C. The travel-time curves for the observed S phases produced by the model are plotted as solid lines in the reversed sections of Figures 3 and 4.

Record sections and the model for line B are shown in Figure 5. The amplitudes of the seismograms have been scaled by distance squared. The first arrivals define several linear segments which are modeled by thin layers with P velocities of 4.63, 5.43 over a thicker layer with a P velocity of 5.94 km/sec. These traveltime curves are offset when they cross two basins along the profile, indicated in Figure 5. Between 10 and 20 km from the CAG quarry, Figure 5A, the profile crosses Boulder Valley and the P2 phase is delayed by 0.2 seconds. Between 18 and 26 km from the CCM quarry, Figure 5B, the Reese River Valley is crossed near Battle Mountain and the P3 phase from CCM is delayed 0.4 seconds. Assuming a valley-fill velocity of 2.0 km/sec, delays of 0.2 and 0.4 seconds correspond to fill thickness of 0.43 and 0.85 km. A reflection, labeled R4 on Figure 5 is visible at distances greater than 35 km and has a similar character as the R4 reflection observed on Line D. This reflection is modeled by an increase in velocity to 6.7 km/sec below the 5.94 km/sec layer. Since line B is not long enough to see the wide angle R5 reflections which would constrain the velocity of 6.7 km/sec, this value was assumed and held fixed. 6.7 km/sec is typical of the velocity found in the lower crust of the other refraction lines in the area. A strong reflection, labeled R5, is visible beyond 60 km for both shotpoints. This reflection constrains the base of the 6.7 km/sec layer at a depth of about 23 km below the surface.

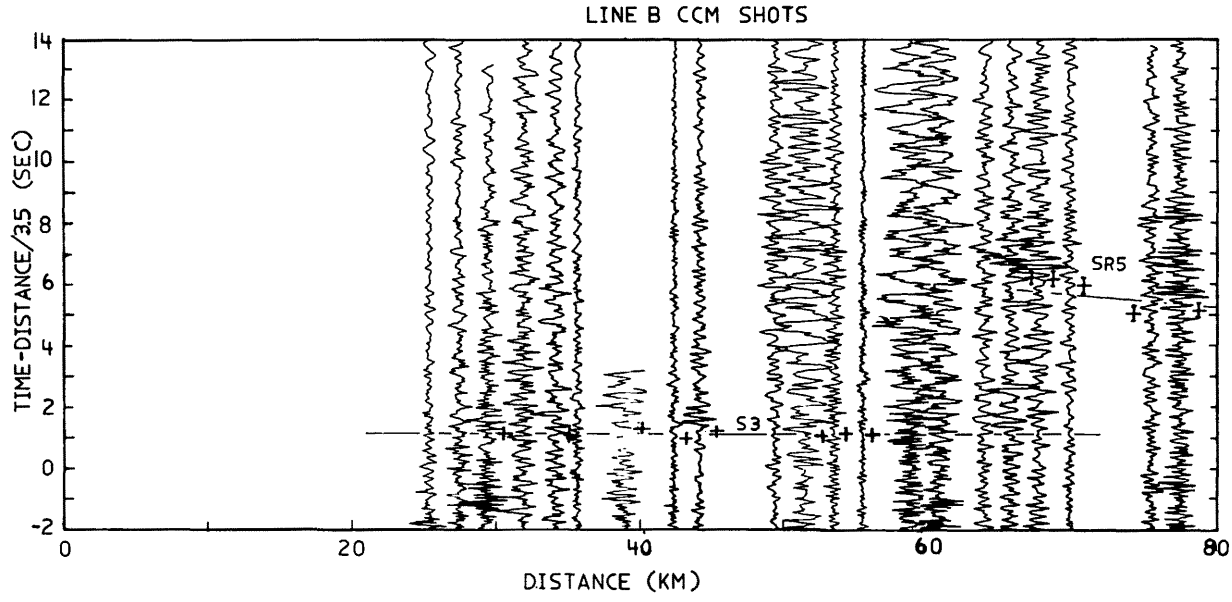

Figure 6. Vertical component record section for CCM shots on line B with a reducing velocity of 3.5 km/sec. S wave travel-time curves are calculated from model in figure 5C.

Low frequency S waves with an apparent velocity near 3.5 km/sec are visible for the CCM shots, S3 on Figures 5B and 6. On Figure 6, a high frequency reflection, SR5, is visible near 70 km at a reduced time near 5 seconds. No S waves were observed on the comperable record section from CAG shots. If these two phases are interpreted as S waves generated at the source, and the layer boundaries are fixed by the P wave travel times, then the upper and lower crustal S velocities are 3.52 and 3.15 km/sec. The average shear velocity of 3.15 km/sec for the lower crust, P velocity of 6.7 km/sec, is unusually low.

Record sections and a model for line A are shown in Figure 7. Amplitudes are scaled to yield approximately constant maximum amplitude on each trace. First arrivals between 10 and 110 km have an apparent velocity of 5.97 km/sec. Between 10 and 60 km the recording sites were located in the sediment filled Reese River Valley. Two stations, one near 21 km and one at 39.5 km were located on bedrock outcrops through the sediment fill. First arrivals at these two stations and for stations beyond 60 km are 0.15 to 0.20 seconds earlier than the stations on the valley fill. Assuming a valley fill velocity of 2.0 km/sec, about 0.32 to 0.42 km of valley fill occupies the Reese River Valley south of CCM. Beyond 150 km, the first arrivals have an apparent velocity of 7.8 km/sec. Starting at 60 km and a reduced time of 2.6 sec a large amplitude reflection with an apparent velocity near 7.8 km/sec is clear and was called the R5 reflection. An abrupt increase in the low-frequency signal at reduced times near 0.0 sec was picked between 180 km and the end of the line and identified as R5 Another reflection, R4, was picked between 9 and 160 km at reduced times near 1.4 sec an with an apparent velocity near 6.0 km/sec. R arrivals between 60 and 90 km are also visibl in Figure 7A. They were based on an increase i the amplitude of the signal except at the tw stations nearest 80 km where the signal leve abruptly decreased at the expected arriva time. This is probably due to destructiv interference between the R4 signal and the coda of earlier arriving phases.

Looking at figure 2, one can see that one c the NTS profiles of Stauber and Boore (1978) coincides with line A between CCM and Austin. The two lines differ in azimuth by about 10 degrees. South of Austin, the two lines diverg more strongly. An expanded view of the line locations around and south of Austin is shown i figure 8. The heavy solid line shows the location of the recording sites for CCM shots which were used to produce the record section i figure 7A. The line between CCM and NTS is shown with a dashed line in figure 8. Recordin sites for NTS events are shown with circles nea the CCM to NTS line. Six sites in the Toquima Range along this line recorded CCM shots and these are shown with triangles in figure 8. Unfortunately, the shot time is not known for the CCM recordings made in the Toquima Range so only apparent velocity information can be extracted from the seismograms. Reduced travel-times from Stauber and Boore (1980) for NTS events recorded on the four profiles indicated in figure 2 are plotted in Figure 9.

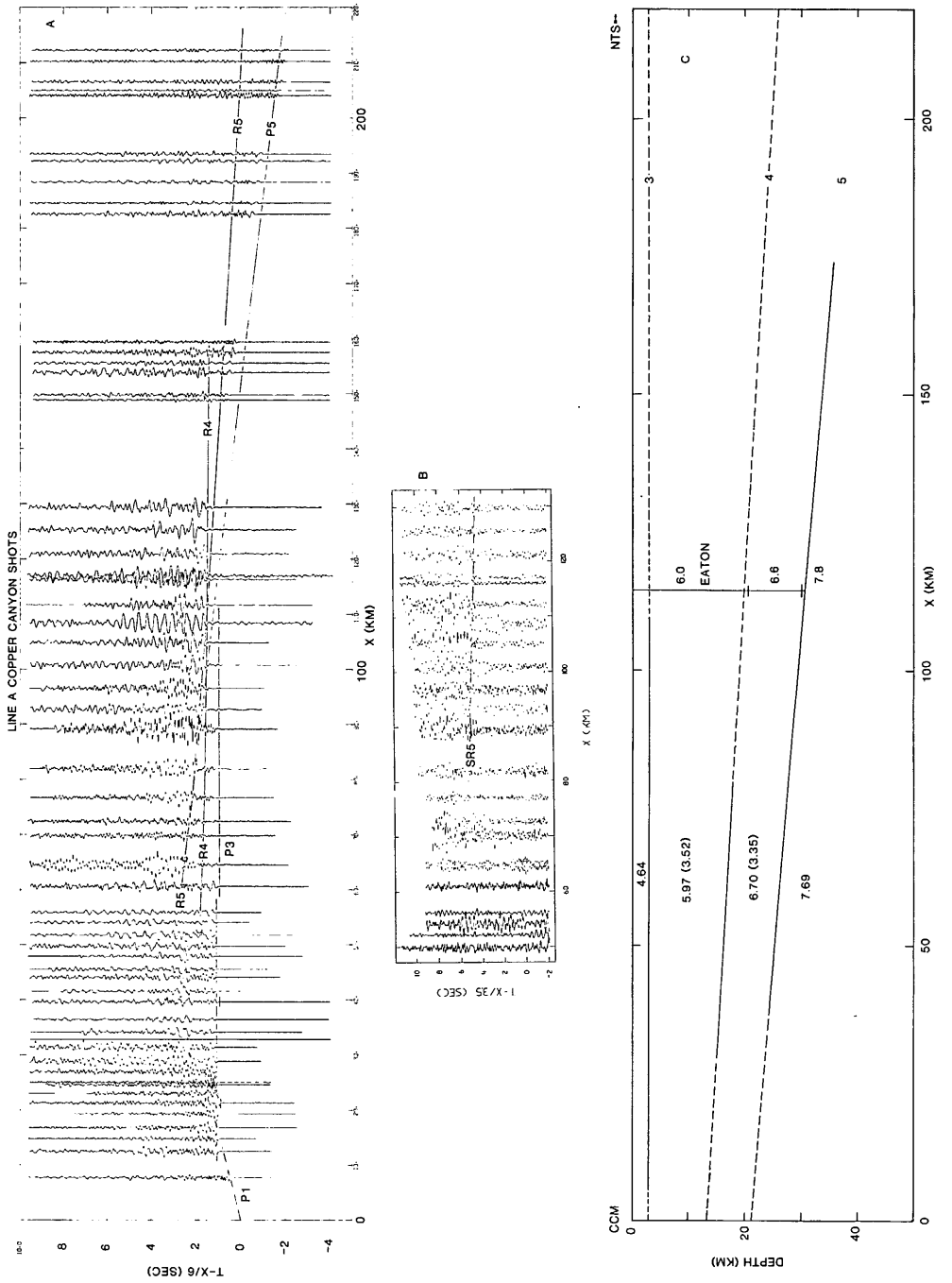

Figure 7. Vertical component record sections and model for line A. Travel-time curves are calculated from model in figure 7C. The reducing velocity for section A is 6.0 km/sec and the reducing velocity for section B is 3.5 km/sec. P and S (in parenthesis) velocities are in km/sec. Velocity model from Eaton (1963) at intersection with line A is shown at vertical bar near 126 km.

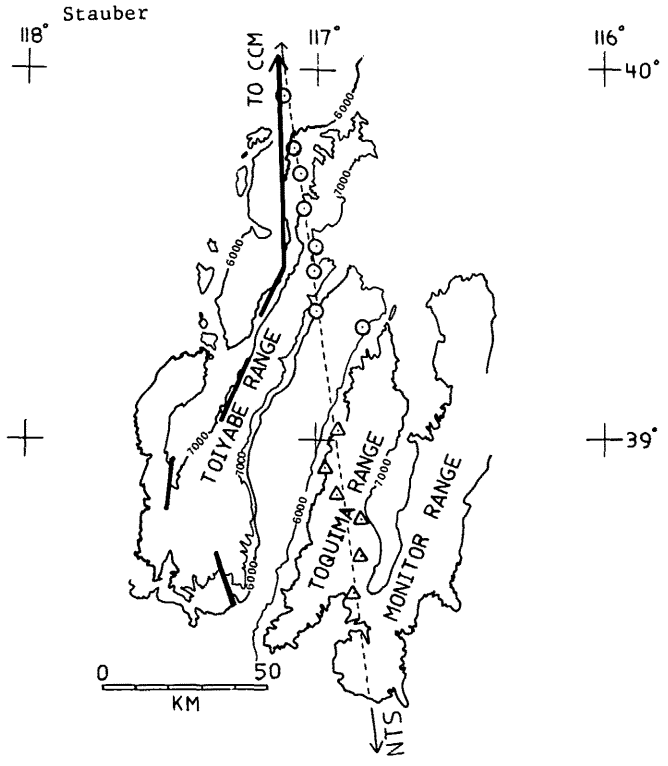

Figure 8. Expanded view of station locations near the southern end of line A. Topographic contours outline the ranges. Heavy solid lines show locations of stations used to produce the record section in figure 7A. Dashed line shows the CCM to NTS line. Stations recording NTS shots are shown as circles and stations in the Toquima Range recording CCM shots are shown as triangles.

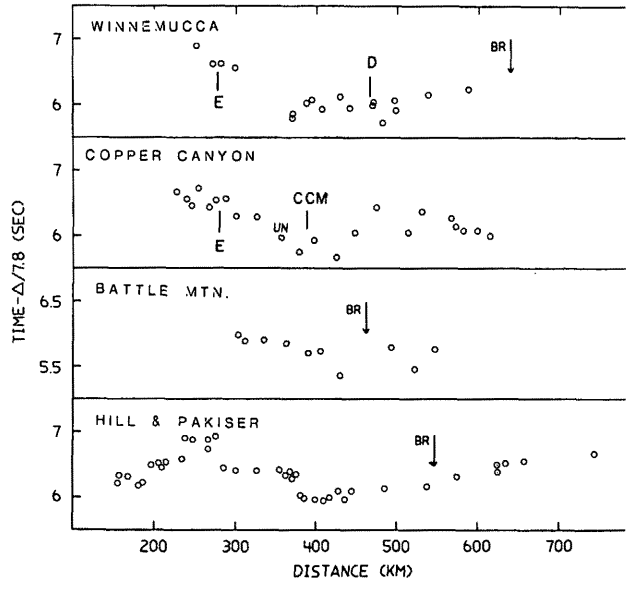

Figure 9. Reduced travel-times for four unreversed NTS profiles reported by Stauber and Boore (1978), labeled S on Figure 2. Locations of intersections with east-west line of Eaton (1963) are indicated by "E" on the Winnemucca and Copper Canyon lines. Intersection of Winnemucca line with line D is indicated with "D" and location of CCM projected onto the Copper Canyon line is labeled "CCM".

The box labeled Copper Canyon in Figure 9 gives the data for the line coinciding with line A. Reduced travel-times, plus an arbitrary constant since the shot time is unknown, for first arrivals from the CCM shot recorded in the Toquima Range are plotted in the top of Figure 10. Six reduced travel-times from the Copper Canyon NTS profile for stations in the Toiyabe Range are reproduced in the bottom of Figure 10.

Treating line A from CCM shots and the Copper Canyon NTS line as a reversed line, ignoring for the moment the differences in location just discussed, and modeling them with dipping planar interfaces results in the model shown in Figure 7C. Like the structure on line D, the fifth interface dips away from CCM. At 126 km, line A crosses the east-west line of Eaton (1963). Eaton's structure is shown on Figure 7C at the intersection with line A, and the agreement is within 1 km in depths of interfaces and 0.1 km/sec in velocities. This is a good agreement, since the structure of Eaton (1963) was not used as a constraint on the inversion of the line A travel-times. The greatest discrepancy between the model and the observations is in the P5 phase from CCM (Fig. 7A). The apparent velocity that fits the first arrival observations between 140 and 220 km is near 7.8 km/sec while the model predicts an apparent velocity of 7.26 km/sec. The discrepancy occurs for probably two reasons. The first is a departure of the fifth interface from the planar surface forced by the modeling technique. A fifth interface which is nearly flat at a depth of 24 km between 0 and 70 km, deepens to about 33 km between 70 and 120 km an stays near 33 km depth for the rest of the line would fit the P5 travel-times on line A more closely The second contributor is the difference in locations of the profiles discussed above. Line A and the Copper Canyon NTS line do not strictly form a reversed profile. Despite these problems, the aggreemen between the models for line A and Eaton's 1963 profile at their intersection is a strong argument for the general validity of the model in Figure 7A.

The real P velocity below the fifth interface can be determined near Austin by usin the data in Figure 10. The stations in the Toiyabe Range recording NTS shots and those in the Toquima Range recording CCM shots provide reversed coverage of a portion of the fifth interface. The apparent velocities resulting from least-square, linear fits give a real velocity below the fifth interface of 7.65 ± 0.11 km/sec, close to the value of 7.69 km/sec obtained from the model in Figure 7C.

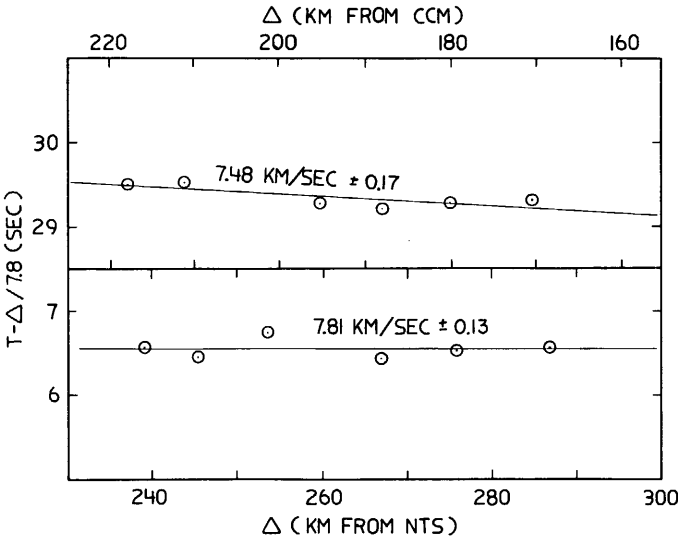

Figure 10. Reduced travel times for stations located along the line between Copper Canyon and NTS. Top panel has times recorded in the Toquima Range for CCM shots. The locations of these stations are shown with triangles on figure 8. The bottom panel has reduced travel times for NTS shots recorded in the northern Toiyabe Range. The station locations are shown as circles in figure 8. Least square linear fits, their slopes and one standard deviation in the uncertainty of these slopes are shown.

Another estimate of the P5 velocity between Winnemucca and Austin can be obtained from the arrival times on the Winnemucca NTS profile, Figure 9. This profile crosses both Line D and the refraction line of Eaton (1963). Using the crustal velocities and thickness from these two cross lines and the travel times from NTS at the intersections, the upper mantle velocity between can be measured. The value that results is 7.73 km/sec. A change in crustal thickness on one of the cross lines of 2 km, within the uncertainty of the determinations, can change the derived velocity by 0.08 km/sec. Uncertainties in the travel times from NTS of 0.10 sec due to the scatter of points, not measurement accuracy, can change the computed velocity by 0.05 km/sec. Therefore, the error in the upper mantle velocity of 7.73 km/sec could be as large as 0.13 km/sec. This value of 7.73 ± 0.13 km/sec is close to the value 7.65 ± 0.11 km/sec obtained near Austin and 7.69 km/sec obtained from the line A model.

A record section was also plotted with a reducing velocity of 3.5 km/sec to facilitate the identification of shear waves (Fig. 7B). The vertical component recordings show a large increase in amplitude between 70 km, 5.5 sec, and 130 km, 4.5 sec. This is probably a near critical-angle shear wave reflection, possibly SR5, the shear wave equivalent of the R5 reflection. The picks are indicated by plus (+) symbols. The solid line shows part of the SR5 travel-time predicted by modeling discussed later. Because of the emergent nature of the SR5 reflection, the picked times are expected to be late and, by inspection of figure 7B, the true arrival times might reasonably be expected to be up to 1.5 sec earlier than the picks.

The travel times of the large-amplitude SR5 arrivals beyond 70 km in Figure 7B were inverted to obtain an average shear velocity in the lower crust along line A. The depth and dip of the interfaces from inversion of the P travel times were held fixed and the S3 shear velocity was held at 3.52 km/sec, the value from line B. The resulting velocity in the lower crust is 3.35 km/sec. This should be considered a minimum since the arrivals are emergent and one expects measured times to be biased toward large values. Subtracting 1.5 sec from all the SR5 travel times, corresponding to the earliest reasonable time, causes the velocity to increase by 0.30 km/sec to 3.65 km/sec. Because no horizontal component records are available, the emergent nature of the arrivals, and possible misidentification of the raypath, I am not confident of the lower crustal shear velocities obtained along lines A and B.

A crustal cross section with a vertical exaggeration of 2.5 constructed from the layered model interpretations of Lines A, B and D is given in Figure 11. The section bends at CCM with the line A structure extending south from CCM and the line D structure extending northwest from CCM. The structure from line B is projected to the cross section at the vertical bar below CCM. P and S velocities, the latter in parenthesis, are shown where determined. The structure proposed by Eaton (1963) is shown at the vertical bar below the location of Austin. The location of the heat flow high, HFH, is shown by the bar at the top. I interpret the region with P velocities greater than 7 km/sec to be mantle. The crust, then, varies in thickness from 34 km at the SE end to 23.5 km near CCM and 30.5 km just SE of QK. This structure confirms the previous interpretations by Stauber and Boore (1978) and Priestly and others (1982) that the early P_n arrivals in northern Nevada are due to a thinning of the crust in the Lake Lahonton depression and not because of an increase in the crustal or upper mantle P velocities.

Using the detailed refraction lines from this study and those of Eaton (1963) and Hill and Pakiser (1966) and the unreversed refraction lines of Stauber and Boore (1978) and Priestly and others (1982), a fairly detailed map of the elevation of the crust-mantle boundary can be constructed for northern Nevada, Figure 12A. To interpolate or extrapolate the crustal thickness, between and around the reversed

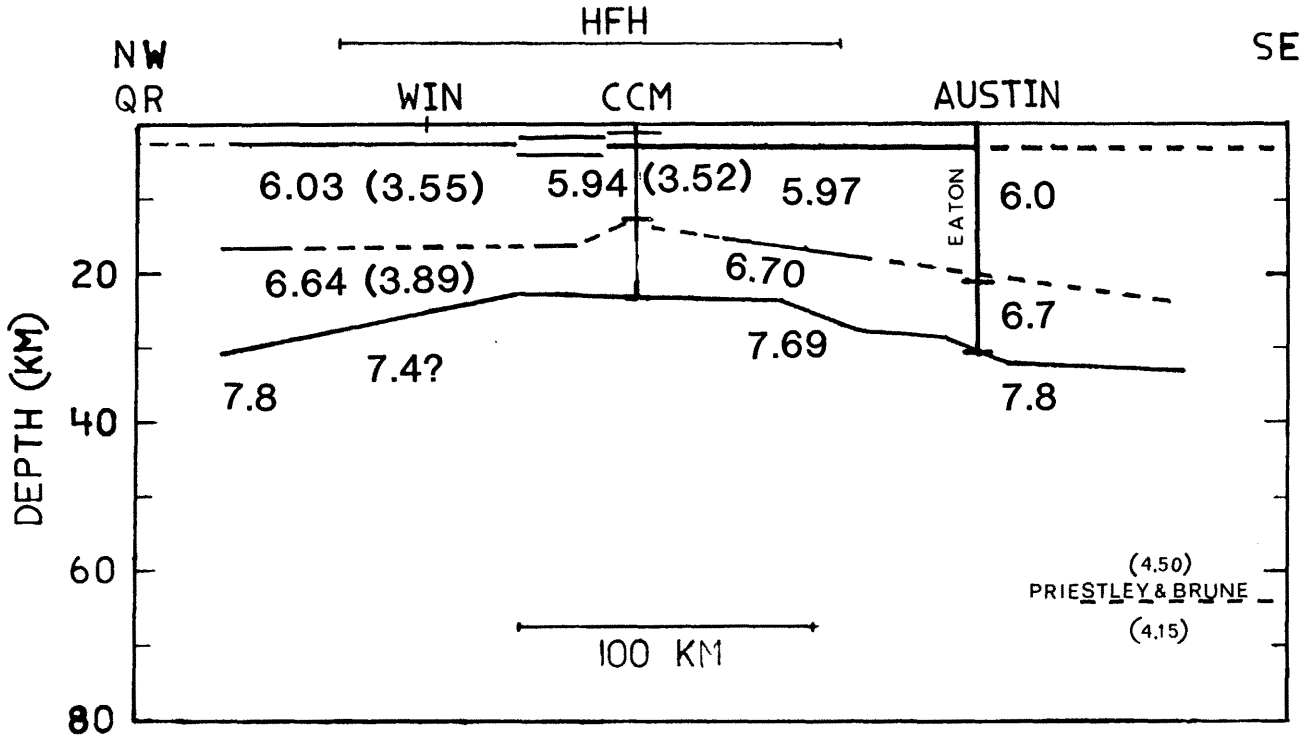

Figure 11. Composite cross section along lines A and D. The profile bends at CCM with the line A model shown to the right and the line D structure shown on the left. The velocity model for line B and Eaton's 1963 line are shown along the vertical lines which mark the intersections of these lines with the cross section. The position of the lithosphere-asthenosphere boundary published by Priestley and Brune (1978) is shown near the southeast end and the location of the Heat Flow high of Lachenbruch and Sass (1976) is indicated with the horizontal bar at the top. WIN marks the position of Winnemucca.

refracton lines using the NTS observations, an upper mantle velocity of 7.8 km/sec was used. Crustal thickness variations were calculated from the deviations in arrival times, from the 7.8 km/sec refraction, by multiplying the arrival time deviations by 10.0 for the four profiles of Stauber and Boore (1978) and by 9.4 for the observations of Priestly and others (1982). The difference in the two constants results in a negligible difference in elevation. The value of 10.0 approximates the case where the relative proportion of upper and lower crust remains constant as the total crustal thickness changes and the value of 9.4 is appropriate when the lower crust maintains a constant thickness. Where the data are sparse the positions of some contours are estimated with the aid of the Bouguer gravity field.

These contours are consistent with the seismic observations, however. The most prominent feature is the shallow crust-mantle boundary in a region extending from Reno to the Battle Mountain-Winnemucca area. The elevations reach as high as -20 km. The elevations decrease to between-30 and -35 km in central Nevada. The pattern coincides with the regional elevation map of northern Nevada, Figure 12C. The areas of thin crust corresponds to a regional topographic low and the thick crust to a topographic high. The crust-mantle elevation map also correlates with the regional Bouguer gravity field, Figure 12B. The gravity field is high where the crust-mantle boundary is shallow and the gravity values are low in central Nevada where the boundary is deep.

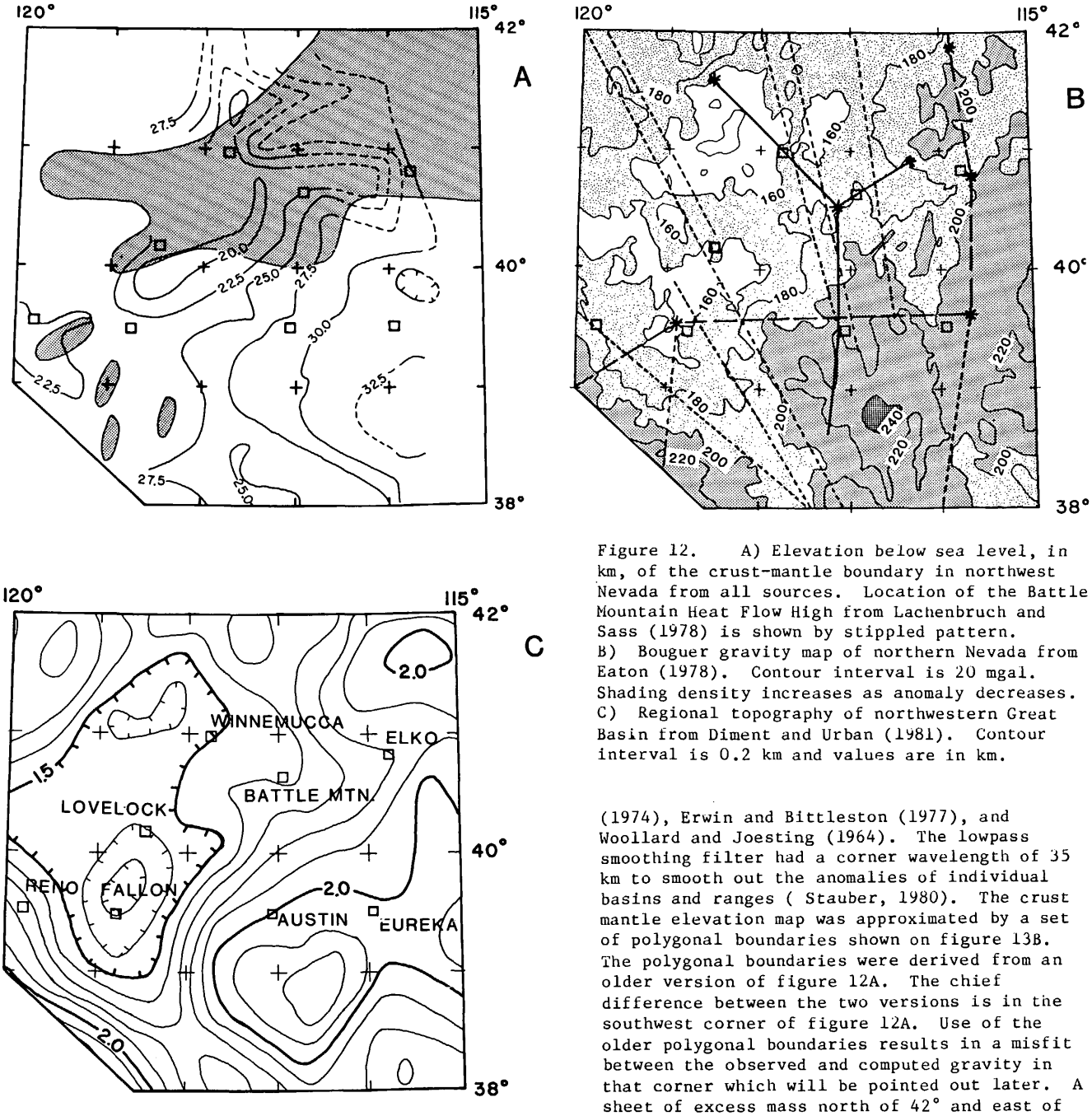

Figure 12. A) Elevation below sea level, in km, of the crust-mantle boundary in northwest Nevada from all sources. Location of the Battle Mountain Heat Flow High from Lachenbruch and Sass (1978) is shown by stippled pattern. B) Bouguer gravity map of northern Nevada from Eaton (1978). Contour interval is 20 mgal. Shading density increases as anomaly decreases. C) Regional topography of northwestern Great Basin from Diment and Urban (1981). Contour interval is 0.2 km and values are in km.

Gravity Field Modeling

Since the regional crustal thickness and gravity maps exhibit the same large scale features it is reasonable to attempt to compare the observed gravity field with the gravity field calculated from the crust-mantle boundary map. This has been attempted by Stauber (1980) for north-central Nevada between 115° and 118° W longitude and 39° and 42° N latitude. A smoothed version of the regional gravity field is presented in Figure 13A. The gravity data used in producing Figure 13A come from Erwin (1974), Erwin and Bittleston (1977), and Woollard and Joesting (1964). The lowpass smoothing filter had a corner wavelength of 35 km to smooth out the anomalies of individual basins and ranges (Stauber, 1980). The crust mantle elevation map was approximated by a set of polygonal boundaries shown on figure 13B. The polygonal boundaries were derived from an older version of figure 12A. The chief difference between the two versions is in the southwest corner of figure 12A. Use of the older polygonal boundaries results in a misfit between the observed and computed gravity in that corner which will be pointed out later. A sheet of excess mass north of 42° and east of 118° was added to approximate the effects of the Snake River Plain structure. The 3-D gravity program of Plouf (1975) was used to compute the gravity anomaly of the polygonal bodies. The gravity program also determined the density contrast for which the computed anomaly most closely matches, in a least-square sense, the smoothed obeserved field (all the polygonal boundaries have the same density contrast) . This density contrast was found to be 0.16 g/cm^3 and the gravity field computed with this contrast is plotted in Figure 13C. The residual field, the difference between the observed field in 13A and the computed field, 13C, is shown in Figure 13D.

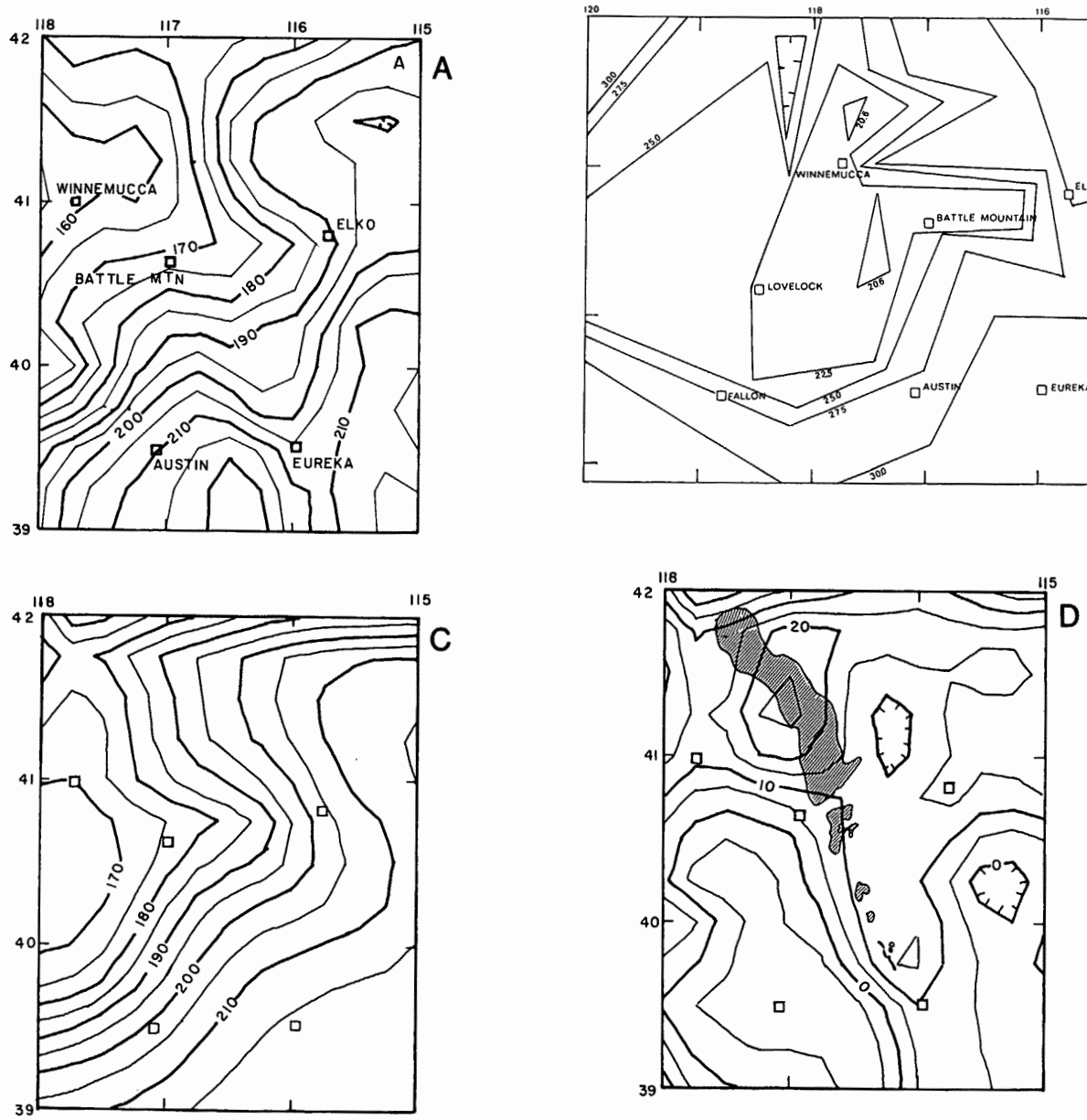

Figure 13 A) Smoothed observed Bouguer gravity field. Contours at 5 mgal intervals.
B) Polygonal boundaries used to approximate crust-mantle boundary topography in figure 12A. Depths are in km.
C) Gravity anomaly calculated from 13B. Contour interval is 5 mgal.
D) Residual gravity field, figure 13A minus 13C. Contour interval is 5 mgal. Outcrops of volcanic rocks associated with the Miocene Northern Nevada Rift, Zoback and Thompson (1978), shown with diagonal hatching.

The computed gravity field, figure 13C, for the polygonal model of Figure 13B which approximates the crustal model presented in this paper is similar to the smoothed observed gravity. The gravity high in the Winnemucca area relative to central Nevada near Eureka in the calculated gravity map is 50 mgal and is 60 mgal for the observed gravity maps. The most obvious residual visible in figure 13D is a NNW-SSE striking ridge of positive residuals coincident with the Miocene Northern Nevada rift zone (Zoback and Thompson, 1978), which is indicated on figure 13D. The gravity high along this rift zone may result from the presence of

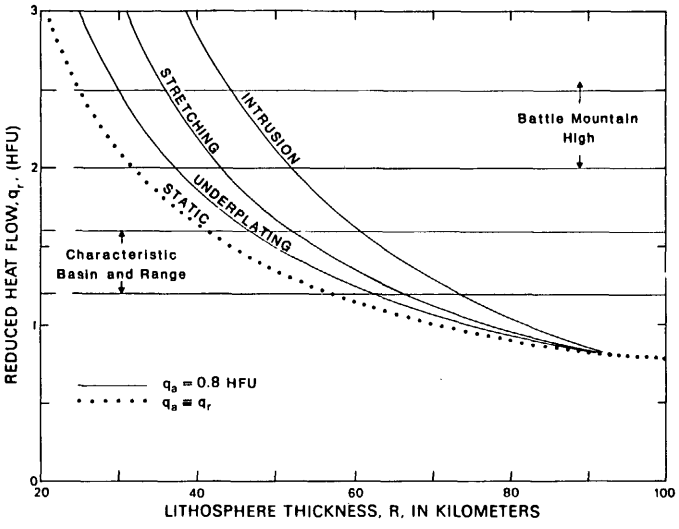

Figure 14. Reduced heat flow vs lithospheric thickness for three models of lithospheric extension taken from Lachenbruch and Sass (1978). Reduced heat flow ranges appropriate for the Battle Mountain heat flow high and normal Basin and Range are indicated.

high density intrusive bodies in the crust which are associated with the Miocene rifting. A steep gradient along the north edge of the residual gravity map probably results from an inadequate representation of the Snake River Plain structure to the north. The north-south striking contours along the southwest edge of the residual gravity map results from the use of the older version of the Crust-Mantle boundary elevation map discussed earlier. Finally there is a gradient resulting in east-west striking contours at about the latitude of Battle Mountain. The width of this gradient zone is comparable to the cutoff wavelength of the smoothing filter used on the gravity data. Because of this one can only say that it's source is shallower than the mid-crust, about 17 km.

The density contrast of 0.16 g/cm^3 is rather small for the density contrast between the crust and mantle. This is especially troublesome since Figure 11 shows that the thickness of the lower crust is relatively constant and the main contrast should be between mantle rocks and upper crustal rocks. One solution to this problem is to postulate a larger density contrast between the crust and mantle and partially compensating low density anomaly below. One candidate is the lithosphere-asthenosphere boundary observed at a depth of 65 km in central Nevada (Priestly and Brune, 1978) and shown in Figure 11. A density contrast of 0.08 g/cm^3 at this boundary (Crough and Thompson, 1976), and a lithosphere thickness 20 to 30 km less in northwest Nevada than in central Nevada would allow a larger, 0.3 to 0.4 g/cm^3, density contrast between the crust and mantle. Thermal-mechanical models for lithospheric extension in the Basin and Range Province proposed by Lachenbruch and Sass (1978) predict relationships between lithospheric thickness, extension rates and surface heat flux. Figure 14, reproduced from Lachenbruch and Sass (1978, Figure 11), shows the relationship between lithospheric thickness and reduced heat flow for three proposed lithospheric extension models. The ranges of reduced heat flow appropriate for normal Basin and Range and the Battle Mountain High are indicated. One can see that the lithospheric thickness decreases with increasing heat flow and that for all three extension modes, the lithosphere could be 15 to 25 km thinner in the heat flow high than in the normal Basin and Range. This is in the range which is consistent with gravity and seismic observations discussed above.

Summary

A combination of unreversed refraction lines utilizing NTS events as sources and reversed refraction lines using quarry blasts and borehole shots results in a roughly north-south crustal cross section across the Battle Mountain Heat Flow High, near Battle Mountian, Nevada, shown in figure 11, and a contour map of the crust-mantle boundary elevation in northern Nevada, figure 12A. The dominant features observed are the area of thin crust coinciding with the Lake Lahonton basin in northwest Nevada and the thick crust occurring in the central part of Nevada. On the profile in figure 11, the heat flow high corresponds to the area of thin crust. The correlation between the spatial extent of the heat flow high, described by Lachenbruch and Sass (1978) shown in figure 2, and the thin crust as shown in figure 12A is not perfect.

The long wavelength Bouguer gravity field correlates well with the topography of the crust-mantle boundary in northeastern Nevada with high gravity values occurring where the crust-mantle boundary is high. If the topography of the crust-mantle boundary is the only source of the Bouguer gravity field, then a low density contrast, 0.16 g/cm^3, between the average crustal and upper mantle densities is required. A larger value for this density contrast is permitted if there is a partly compensating density contrast at another boundary having a long wavelength shape similar to the crust mantle boundary. One possible boundary is the lithosphere-asthenosphere boundary which occurs at about 65 km depth in central Nevada (Priestley and Brune, 1978). The magnitude of the gravity high observed in the area of thin crust could be explained by a lithosphere-asthenosphere boundary which is 20 to 30 km higher in the Lake Lahonton basin than in central Nevada and a larger, 0.3 to 0.4 g/cm^3 instead of 0.16 g/cm^3 density difference between the average crustal and the

upper mantle densities. Further three dimensional gravity modeling using the updated crust-mantle elevation map of figure 12A, which covers a larger region of northwestern Nevada, the observed Bouguer gravity field over this larger region, and including upper mantle density variations such as topography on the lithosphere-asthenosphere boundary is necessary to make this discussion more quantitative. Since thermal-mechanical models of lithospheric extension such as those proposed by Lachenbruch and Sass (1978) predict relationships between lithospheric thickness, extension rates, and heat flow, more extensive gravity modeling of the upper mantle in northwest Nevada is likely to yield useful constraints on the extension mechanism of the lithosphere in this region.

Acknowledgements

This work was funded by N.S.F. grant number EAR75-04291 A02.

References

Criley, E. and Eaton, J., 1978, Five-day recorder seismic system,U. S. Geol. Surv., open file report, No. 78-266.

Crough. S. T., and G. A. Thompson, 1976, Thermal model of continental lithosphere, J. Geophys. Res., v. 81,p. 4857-4861, 1976.

Diment, W. H., and T. C. Urban, 1981, Average elevation map of the conterminous United States (Gilluly averaging method), Geophysical Investigations Map GP-933, 1:2,500,000 , U.S. Geological Survey.

Eaton, J. P., 1963, Crustal structure from San Francisco, California to Eureka, Nevada, from seismic-refraction measurements, Jour. Geophys. Res., v. 68, p. 5789-5806.

Erwin, J. W., 1974, Bouguer Gravity map of Nevada Winnemucca sheet, Nevada Bureau of Mines and Geology, Map 47.

Erwin, J. W. and Bittleston, E. W., 1977, Bouguer gravity map of Nevada Millet sheet, Nevada Bureau of Mines and Geology, map 53.

Hill, D. P. and Pakiser, L. C., 1966, Crustal structure between the Nevada Test Site and Boise, Idaho, from seismic-refraction measurements, Amer. Geophys. Union Monograph 10, p. 391-319.

Lachenbruch, A. H., Sass, J. H., 1978, Models of an extending lithosphere and heat flow in the Basin and Range province, Geophys. Soc. Am., Memoir 152, p. 209-250.

Plouff, D., 1975, Derivation of formulas and FORTRAN programs to compute gravity anomalies of prisms, U.S. Geological Survey Report, USGS-GD-75-015.

Priestley, K., Brune, J., 1978, Surface waves and the structure of the Great Basin of Nevada and western Utah, J. Geophys. Res., v. 83, p. 2265-2272.

Priestley, K. F., A. S. Ryall and G. S. Fezie, 1982, Crust and upper mantle structure in the northwest Basin and Rance Province, Bull. Seis. Soc. Am., v. 72, p. 911-923.

Stauber, D. A. and Boore, D. M., 1978, Crustal thickness in northern Nevada from seismic refraction profiles, Bull., Seis. Soc. Am., 68, v. 1049-1058.

Stauber, D. A., 1980, Crustal structure in the Battle Mountain Heat Flow High in northern Nevada from seismic refraction profiles and Rayleigh wave phase velocities, PhD thesis, Stanford University.

Woollard, G. P. and Joesting, H. R., 1964, Bouguer gravity anomaly map of the United States, Am. Geophys. Union, Special Committee for Geophysical and Geological Study of the Continents, G. P. Woolord, Chairman, and the U. S. Geological Survey, H. R. Joesting, Coordinator.

Zoback, M. L. and Thompson, G. A., 1978, Basin and Range rifting in northern Nevada: Clues from a mid-miocene rift and its subsequent offsets, Geology, v. 6, p. 111-116.